FGM Stainless steel-Ti(C,N) cermets through colloidal processing

J.A. Escribano (a), J.L.García (a), P. Alvaredo (b), B.Ferrari (a), E. Gordo (b), A.J.Sanchez-Herencia (a)

(a) *Instituto de Cerámica y Vidrio, CSIC, c/Kelsen 5, 28049 Madrid, Spain*

(b) *Department of Materials Science and Engineering, University Carlos III, Avda. Universidad 30, 28911 Leganés, Madrid, Spain*

Abstract: In this work, the colloidal approach was used to promote a gradation in the composition of a cermet, based on the mixture of stainless steel and Ti(C,N) during powder consolidation into a bulk part. The colloidal processing of non-oxides in aqueous media requires an elevated control over the evolution of the surface chemistry of the powders, in order to obtain stable and high concentrated slurries of the mixture of metal/non-oxide ceramic. The advantage of those methods lies on the fabrication of complex micro-architectures where the second phases are intimately and homogeneously dispersed in the microstructure of the composite. Moreover, those techniques allow the processing of fine particles with low compressibility and flowability which difficult conventional powder metallurgical processing. The results shown in this work evidence the feasibility of obtaining continuous functionally graded materials (FGM) through slip casting in porous molds, as well as the relevance of the rheological properties of the composite slurries on the final characteristics of the material.

Keywords: Ti(C,N), Cermets, Colloidal processing, Functionally gradient material, Steel

1. Introduction

The FGMs are composites in which the concentration of the components continuously varies within the compact from one side to the other. Changes in composition provide a gradient of specific properties, which can improve the compatibility between pure phases, such as metals and ceramics, or inhibit damage or crack propagation [1]. This is why the FGMs are useful structures for thermal barriers, armor, cutting tools, and biomedical applications. There are numerous techniques to manufacture FGMs as a function of the requirements for raw material and final properties [2]. The variation on the composition can be forced through a succession of layers of different microstructures, for example by the film deposition techniques or varying the powder composition on the press die in PM, which leads to a non-continuous graded material with very well defined interfaces between layers. However, a continuous graded material can be only generated causing the migration or diffusion of a component through the microstructure. Those continuous structures prevent residual stresses, emerging at the interfaces of layered structures due to the mismatch between thermal expansion coefficients of joined phases that many times are the cause of the whole structure failure.

Among the fields of application, the FGM structures are especially useful in the fabrication of cutting tools [3–5]. This is because of the gradual increment of the concentration of the reinforcing phase along the structure, ending in a full consolidated ceramic layer, will increase the mechanical strength and the wear resistance of the tool while maintaining the structural stability provided by the cermet to the whole structure [6,7]. Regarding the Ti(C,N)-based cermets, there are several examples in which a FGM structure is generated in the area near the surface using N and Co as metallic phase. The most commonly used method for this is the melt metal infiltration [8,9] or by diffusional processes induced by a reactive gas phase [6,10]. Techniques based on colloidal processing are proposed in this work, as the successful application of the colloidal techniques would allow the one-step shaping of the FGMs, without intermediated compaction steps such as preform fabrication, metal fusion or infiltration, or combined thermal cycles.

Colloidal processing techniques are widely employed in the ceramic field, which have been probed to provide better dispersion of the phases and higher control of the microstructures [11,12]. These advantages have been tested for the processing of Fe based cermets [12] with the aim to achieve effective microstructures, through a very intimate mixture of the ceramic and metal phases, using very fine powder particles and avoiding mechanical milling. The colloidal processing implies the formation of suspensions in aqueous media, which is a drawback in the case of both non-oxide ceramic and metal particles, due to the elevated reactivity of these materials with the suspension media. From an electrochemical point of view, water is one of the more complex liquid media to work with. It has a very high polar moment which requires to extreme the control of the conditions of the suspensions [13–15] to prevent the particle oxidation, while maintaining the interparticle repulsion networks and then the suspension stability. Beyond the

* Corresponding authors. Tel.: +34 917355840.
  E-mail address: jescribano@icv.csic.es (J.A. Escribano).

superficial stability of the particles within the dispersions, a main requirement in the colloidal shaping of slurries is the adjustment of their flow conditions. The rheological behavior of the high concentrated suspensions or slurries should allow the homogeneous mixture of both phases, as well as avoid the segregation during the processing of the compact. All the requirements imposed to the formulation of slurries can be faced by the employment of different water compatible organic additives or dispersants which, besides improving the rheological behavior of the slurry, impede the oxidation of both matrix and reinforcement. Both, the fluidity of the slurry and the high relative mobility of the particles within it, contribute to extend the microstructural design to complex micro-architectures, such as multilayers, coatings and functional graded materials (FGM), depending on the colloidal processing technique used to shape the bulk pieces [16].

The objective of this work is the formulation of stable suspensions of a mixture of stainless steel powder and Ti(C,N) particles and the study of the rheological properties in order to process a FGM. The aqueous dispersion of an AISI 430L stainless steel and Ti(C,N) powder with polyethylenimine (PEI) has been studied. In order to characterize the FGM structure, bulk materials with different 430L/Ti(C,N) ratios from 50/50 to 30/70 v/v have been prepared by slip casting using a porous cast.

2. Experimental

2.1. Materials

The raw materials used in this study were a stainless steel (grade 430L) powder (Sandvick, Sweeden) with a surface area of 1 m^2/g and a density of 7.7 g/cm^3, and a Ti(C,N) powder (H. C. Stark, Germany) with a surface area of 3 m^2/g and a density of 5.1 g/cm^3. Surface area was determined by Monosorb Surface Area (Quantachrome Corporation, USA) and density by Monosorb Multipycnometer (Quantachrome Corporation, USA).

Particle size was determined by Mastersizer S (Malvern instruments Ltd., USA), while zeta potential measurement was done using Zetasizer Nano ZS (Malvern, UK). For the determination of the electrokinetic behavior of the 430L and Ti(C,N) powders in aqueous media, suspensions were prepared at 0.1 g/L in 10^{-2} M KCl, using HTMA and HNO_3 to adjust the pH. A 0.4 wt.% of the content of solids of polyethylenimine (PEI) with high molecular weight (>25,000 KDa, Sigma-Aldrich,Germany) was added as dispersant.

2.2. Suspension preparation

The high solid content suspensions were formulated using water as dispersion media. The slurries were prepared in deionized water with HTMA to adjust the pH up to 10–11, where ferrous surfaces are chemically stable, then 0.4 wt.% of PEI was added as dispersant. The Ti(C,N) and 430L slurries were prepared separately and milled in a ball mill for 1 h, using Si_3N_4 and nylon balls, respectively. After milling, monophasic slurries were mixed to fit three different compositions: 430L/Ti(C,N) 50/50 v/v (50TiCN), 430L/Ti(CN) 40/60 v/v (60TiCN) and 430L/Ti(CN) 30/70 v/v (70TiCN). The composite slurries, as well as 100% 430L (430L) and 100% Ti(C,N) (TiCN) slurries, were considered for the study of rheology. To measure the rheology, a Haake Mars rheometer (Thermo Scientific, Germany) with a double-cone plate fix of 60 mm of diameter and an angle of 2° (DC60/2°) was used. Tests were performed in a control rate mode (CR) shearing from 0 to 1000 s^{-1} in 2 min, dwelling at 1000 s^{-1} for 1 min and shearing down to 0 s^{-1} in 2 min and control stress from 0 to 6 Pa in 2 min and down to 0 Pa in the same time. All tests were done at a constant temperature of 23 ± 0.5 °C. The applied high-shear rates during up-ramps are enough to achieve a reproducible suspension microstructure, dependent only on the suspension composition, but not on the slurry preparation history [17]. Then the flow curves presented

are the down-ramps in the log–log plot and fitting following the Cross model (1):

$$\eta = \eta_\infty \frac{\eta_0 - \eta_\infty}{1 + (C)^n} \tag{1}$$

where η_0 and η_∞ are the extrapolation of the viscosity to zero and infinity respectively, C is a time constant and n is the rate constant, and it is a parameter which is related with the dependence of viscosity on the shear rate. The Cross model describes the limit behavior of the standing suspension and at an infinite shear rate, therefore not only gives information about which suspension is more viscous but which is more stable.

In order to describe the rheological behavior of the slurries, the other model used was the Casson model:

$$\sigma^{1/2} = \sigma_0^{1/2} + (k\dot{\gamma})^{1/2} \tag{2}$$

where σ is the shear stress, σ_0 is the yield stress and k is the consistency. This model describes the flow curves of shear thinning slurries and allows calculating the yield point, σ_0, which is the value of the shear from which the suspension starts to flow.

2.3. Preparation of the biphasic monolithic and functionally graded materials

Composite slurries were casted on using a porous alumina cast and a plastic mold. The FGM microstructures were shaped by applying an intense magnetic field during casting of the 50TiCN slurries. The magnet used was a neodymium magnet (NdFeB) parallelepiped shaped with dimensions of 2 × 1 × 0.5 cm and 1.5 T on the surface. The suspensions were placed in a cylindrical plastic mold and slip-casted using a porous cast with a magnet attached as shown at the scheme of Fig. 1. The magnet was removed after a certain time (from 20 min to 15 h) and the dry green pieces were then characterized and sintered to evaluate the separation between phases.

2.4. Characterization of the cermets

Casted samples were sintered at 1450 °C for 60 min in vacuum (10^{-5} atm) [18]. The micrographs of the green pieces were recorder using a T-100 scanning electron microscopy (Hitachi, Japan). The density of the compacts was measured using an Accupyc He Pycnometer (Micrometrics, USA), and relative densities were calculated using the mixtures law using the value of as-received powder densities determined also by pycnometry as described above. The open porosity of the FGM slides was determined by water immersion using the "*Standard test method for water absorption, bulk density, apparent porosity and apparent specific gravity of Fired Whiteware Products*" (ASTM C373-88) through Eq. (3), where P is the open porosity, M is the mass of the water-saturated sample, D is the mass of the dry sample, S is the mass of the sample immersed in water and ρ_{H_2O} is the density of the water at the experiment temperature.

$$P = \frac{M - D}{M - S} \cdot \rho_{H_2O} \cdot 100 \tag{3}$$

The microstructure of the sintered samples was registered using a XL-30 scanning electron microscope (Philips, Netherlands). The hardness of the sintered compacts was measure by Vickers method with 30 kg load, making 7–10 indentations per sample. The hardness values shown in this paper have a standard deviation of ± 10. The image analysis was carried out by using Image J software (National Institute of Health, USA) using 5 micrographs of 160 × 120 μm per sample.
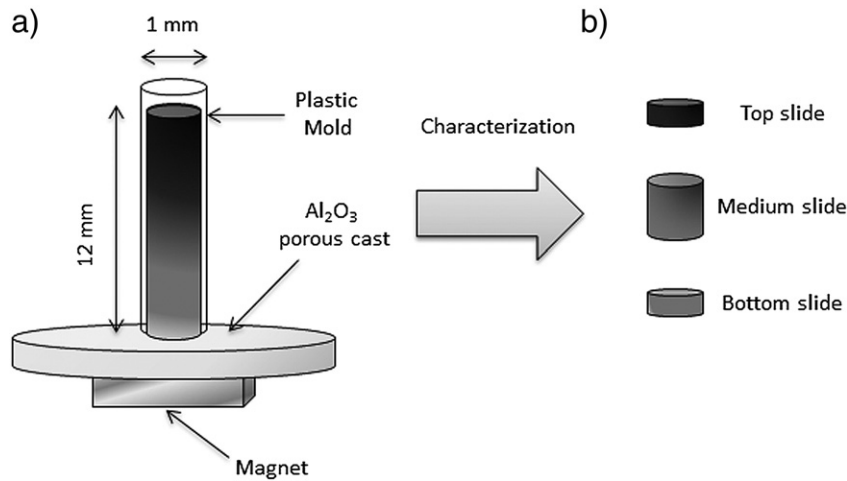
Fig. 1. a) Scheme of the preparation of FGM and b) slides for the characterization of the FGM.

3. Results and discussion

3.1. Chemical and colloidal stability

In powder processing, both the mean particle size and its distribution are crucial parameters to consider. The particle size distributions for 430L and Ti(C,N) powders are shown in Fig. 2. Both powders present a wide fraction of fines. Both mono-modal distributions are skewed to the right leading to maximum particle sizes of 30 μm and 9 μm for 430L and Ti(C,N), respectively. The mean diameter (dv50) of the 430L powder is 11 μm, while the Ti(C,N) powder has a dv50 of 2 μm, being one order of magnitude smaller than the 430L powders. Moreover the 95 vol.% of the particles in the 430L powder is over 2 μm, when a 20 vol.% of Ti(C,N) is within the submicronic range (0.2 μm < dv < 1 μm). Such a wide fraction of fines in Ti(C,N) powders, with its irregular morphology [12], will determine the slurry flux during casting.

The major difficulty in the processing of metal and non-oxide powders in water is to control the chemistry of their surfaces. In the case of metals, it is crucial to avoid the massive oxidation and corrosion of particles. The chemical stabilization of Fe has been described in a previous work [12]. The oxidation of the Fe powder could be limited to the formation of a passivation layer on the surface of the particle at alkaline pH values, which protects the core of the particle against oxidation. A similar study was developed for the 430L and its principal alloying element: the Cr. Similarly that occurs with Fe: a stable layer of Fe_2O_3 is formed on the surface of 430L particles promoting its passivation at basic pH. The contribution of the Cr to the chemical stability of the 430L powder in an aqueous medium results in the stabilization of the surface at acid pH values by forming a layer of Cr_2O_3.

The colloidal behavior of the suspensions was characterized by the determination of the zeta potential of 0.1 g/l suspensions. In Fig. 3, the plot shows the variation of the zeta potential versus pH for 430L and Ti(C,N) bare-powders and when PEI is added as dispersant.

As seen in Fig. 3, the zeta potential of the 430L powder is negative in all the pH range, obtaining the maximum particle charge at pH 11. Meanwhile, the Ti(C,N) presents an isoelectric point (IEP) at pH 2.4. At lower pH values than the IEP, the Ti(C,N) surface is positively charged, and above the IEP it becomes negative. Notice that both powders have a negative zeta potential of 35–40 mV in an absolute value when pH ranges between 10 and 11. At this point, the 430L will preserve its passivation layer, while the surfaces of both powders are able to adsorb a cationic polyelectrolyte as the PEI. The colloidal behavior of the 430L and Ti(C,N) powders when their surfaces are modified at pH 10–11 by adsorbing a 0.4 wt.% of PEI was also shown at the plot. The adsorbed PEI changes the charge of the surfaces turning them positive in almost all the pH range.

The PEI is a cationic additive which contains primary, secondary, and tertiary amino groups ($-NH_x-$) in the ratio of 1:2:1, and it presents the particularity of maintaining a certain positive charge at elevated pH [19]. Therefore the positively charged PEI is efficiently adsorbed on the negatively charged surfaces. This kind of additives, the polyelectrolytes,
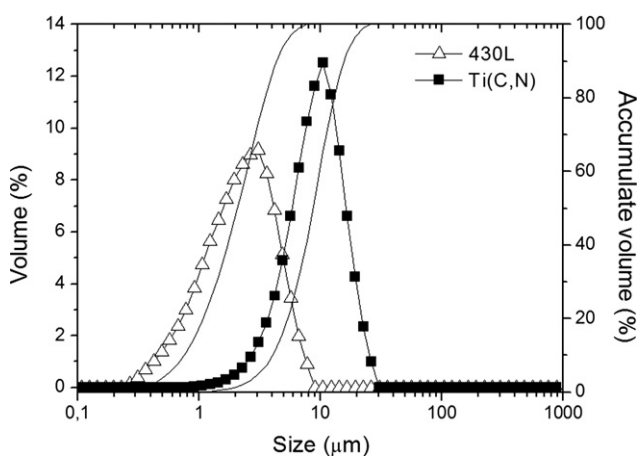

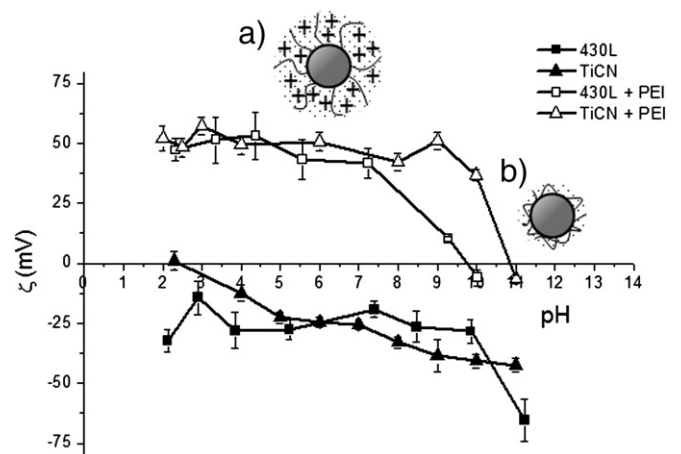**Fig. 2.** Particle size distribution of the 430L and Ti(C,N) powders.

Fig. 3. Zeta potential evolution vs pH of the 430L and Ti(C,N) with and without PEI adsortion, and the schemes of a) Tail and b) Train conformation of PEI over the particle surface.
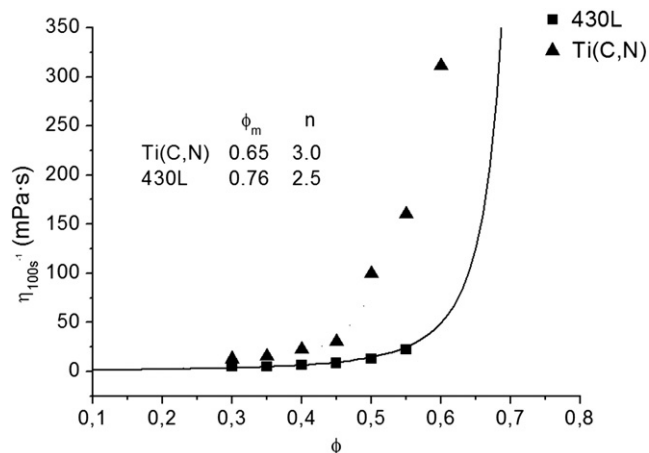
Fig. 4. Evolution of the viscosity vs the volume fraction of the 430L and TiCN slurries. The table in the inset summarizes the main parameters of the Krieger–Dougherty approach.

usually stabilizes the suspensions by an electrosteric mechanism through which their lateral charges aid in the dispersion ("tail" conformation in scheme (a) at Fig. 3), where the volume that they occupy on the particle surfaces prevents contact between them. However, the lower charge registered at pH 10–11, when PEI adsorbs, evidences that the PEI conformation on the surface is the "train" type (scheme

(b) in Fig. 3) [20]. This conformation of the dispersant onto the particle surface promotes the multipoint adsorption, which develops a strong additive–particle anchoring while provides the particles with a mainly steric repulsion mechanism. In this conformation, the organic chains are retracted over the surface and then facilitate the suspension flow. In those cases, the packaging degree improves, because of the volume occupied by the polymer is very low and then it allows a better approaching of the particles during shaping. Taking into account the chemical and colloidal stability of both powders, high solid content slurries of 430L and Ti(C,N) powders were formulated at pH 11 adding 0.4 wt.% of PEI.

3.2. Dispersion and rheological behavior of composites with different 430L/Ti(C,N) rates

The solid content of monophasic slurries was optimized in terms of rheology. In the microstructure of a slurry, the distance between the particles decreases when the solid content increases, causing an increment of the particle–particle interactions which difficult the flow [17]. There is a direct relationship between the packing density of the monolithic and the flow behavior of the slurry. In order to process dense materials slurries should contain the maximum possible amount of powder in suspension, keeping an adequate viscosity for casting. In order to select the optimal solid content to formulate the slurries, the flow curves of the TiCN and 430L suspensions were recorded when the solid content
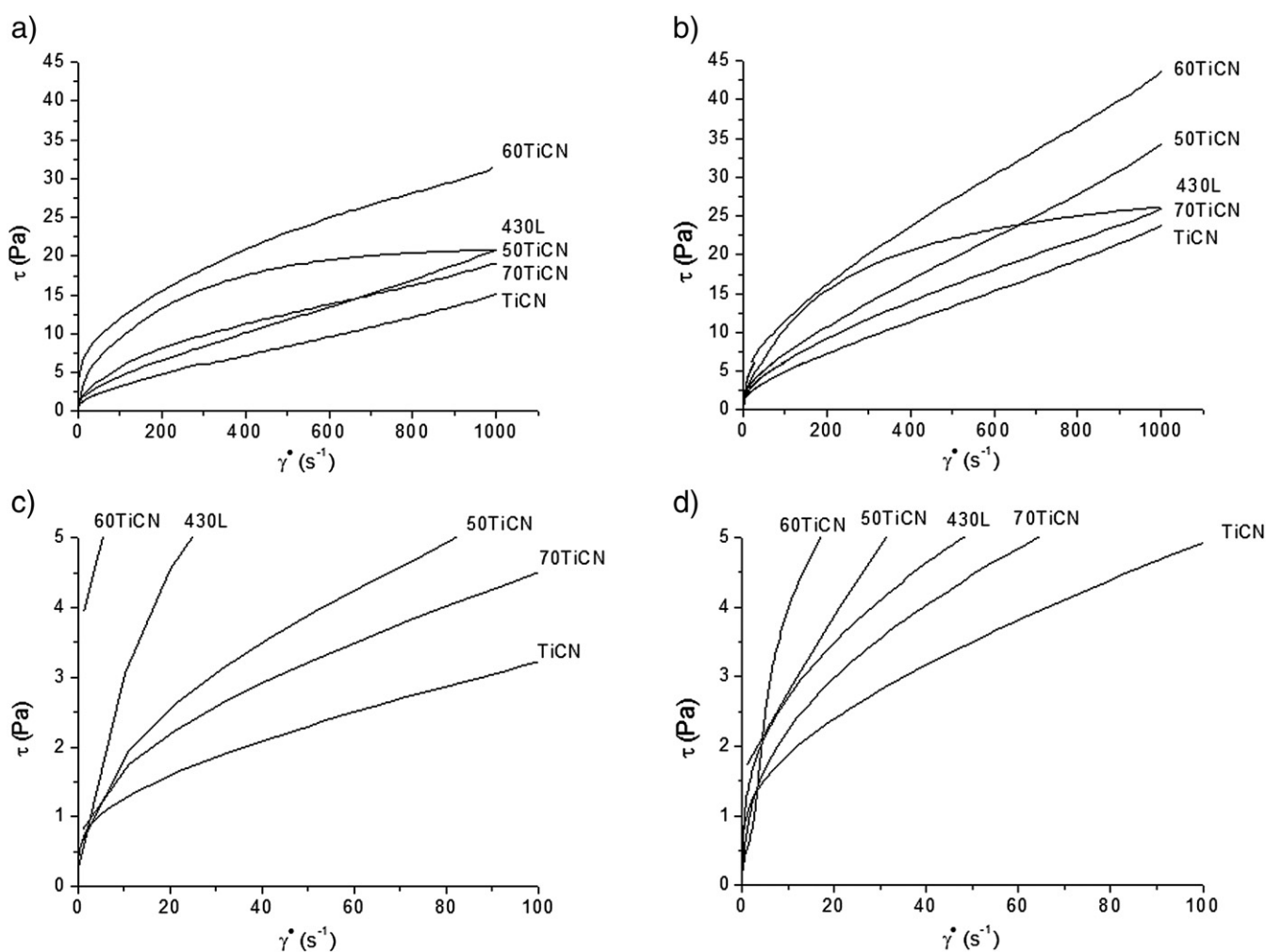

Fig. 5. Flow curves measured in controlled shear and control stress mode of suspensions prepared at 45 vol.% (a and c) and 50 vol.% solid loadings (b and d), respectively.

Solid loading	45 vol.%				50 vol.%			
Composition	σ_0	η_0	η_{100s-1}	η_∞	σ_0	η_0	η_{100s-1}	η_∞
	Pa	Pa s	mPa s	mPa s	Pa	Pa s	mPa s	mPa s
Ti(C,N)	0.59	4.78	31	14	0.78	9.17	48	18
70TiCN	0.66	2.04	45	14	0.56	3.35	62	17
60TiCN	5.84	9.16	119	35	3.65	9.74	114	3
50TiCN	1.02	0.89	57	4	0.92	9.64	72	3
430L	4.37	3.36	85	<1	1.71	39.79	128	18

increases from 30 up to 57 vol.%. Fig. 4 shows the variation of the viscosity for a shear rate of 100 s^{-1} versus the volumetric solid fraction $(0.30 < \phi < 0.60)$ of the Ti(C,N) and 430L slurries.

The results plotted in Fig. 4 correspond to a distribution described by the modified Krieger–Dougherty model (Eq. 4), which allows predicting the maximum packing fraction (ϕ_m) achieved for a dispersed and stabilized suspension of particles.

$$\eta = \left(1 - \frac{\phi}{\phi_m}\right)^{-[\eta]\phi_m} \qquad (4)$$

where η is the relative viscosity at 100 s^{-1} and $[\eta]$ is the intrinsic viscosity. The $[\eta]\phi_m$ exponent is commonly substituted by n which is a value dependent on the shape of the particles. For both systems, the adjusted parameters of the Krieger–Dougherty model are included at the inset in Fig. 4.

As can be observed in the plot, a higher solid content can be achieved for the spherical 430L powder $(\phi_m = 0.76)$ than for the irregular Ti(C,N) particles $(\phi_m = 0.65)$. Maximum packing fraction calculated from experimental data of viscosity even exceeds the random close packing calculated for spherical particles $(\phi_m = 0.64)$ for both slurries [21]. This is mainly due to the wide particle size distributions shown in Fig. 2. So we can estimate that, in our slurries, the fine particles can fulfil the holes among the coarse particles providing a closer packed structure in the monolithic than theory predicts for a monomodal distribution of spherical particles. In order to establish the relationship between rheology and packing degree in the colloidal processing of the 430L/Ti(C,N) cermets, two different solid contents (45 vol.% and 50 vol.%) were selected to prepare monophasic (TiCN and 430L) and biphasic (50TiCN, 60TiCN and 70TiCN) monolithic bulk pieces.

Plots a and b in Fig. 5 show the flow curves for the slurries with solid loadings of 45 and 50 vol.%, respectively measured in control rate mode,
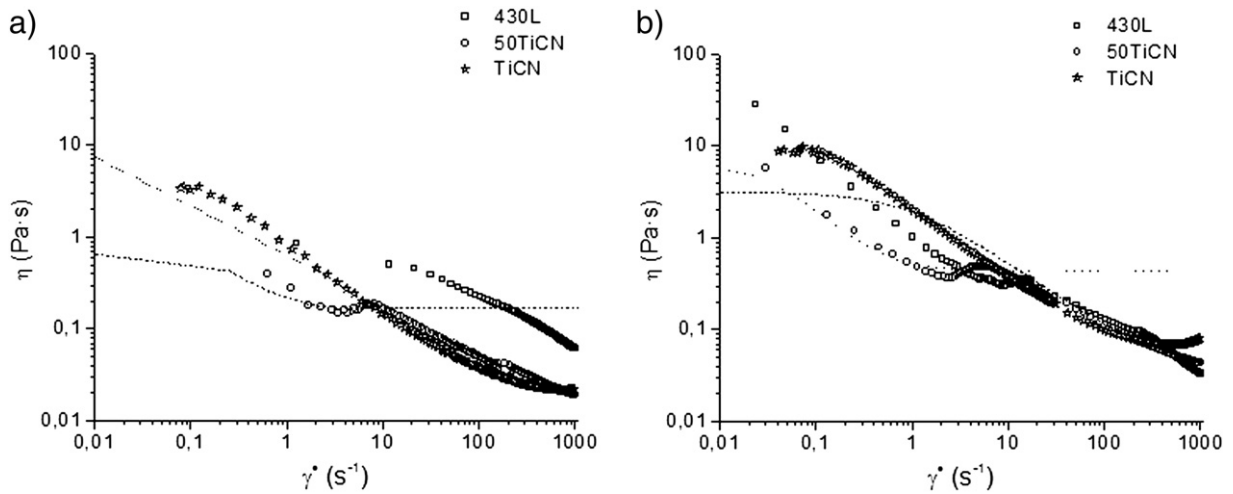
and plots c and d are respectively the flow curves measured in control stress mode. All the curves present hysteresis. In order to determine how the microstructure of the suspension evolves when the reinforcing phase (Ti(C,N) powder is introduced, a pre-shearing of 1000 s^{-1} for 1 min was applied in all cases, and then only the down curves are plotted [22]. Table 1 collects, among others parameters, the yield stresses (σ_0) of the slurries.

As can be observed in the Fig. 5, the flow curves of 430L present a shear thinning behavior for both solid loadings, while the TiCN slurry exhibits a slight shear thickening behavior at high-shear rates. The shear thickening behavior is usually typical for materials with crystalline anisotropy which develop different charges in surface edges and faces (for example kaolin and ZnO), but in our case this slurry performance is due to the irregular morphology of the Ti(C,N) particles.

The 430L slurry shows a pseudoplastic behavior with a relatively high yield point $(\sigma_0 = 4.37$ Pa and 0.59 Pa, for the 45 and 50 vol.% slurries, respectively, determined by the Casson model, Eq. (2)). The σ_0 is always higher for the suspension of 430L than for TiCN (4.37 Pa and 0.59 Pa respectively). Therefore the structures formed within the suspensions of 430L are stronger than for TiCN powders. As the ceramic reinforcement is added, fewer 430L structures are formed so σ_0 decreases, with the exception of the 60TiCN suspensions that exhibit an anomalous behavior. When the solid volume fraction increases to 50 vol.%, the value of σ_0 increases but the trend of the rheological behavior is retained when the ceramic phase is added. Both features, thickening at high shear rates and the pseudoplastic behavior, are characteristic of the ceramic (TiCN) and the metal (430L) slurries, respectively. When the volume of the ceramic phase increases in the fraction of solids, the flow curves reflect it: the σ_0 decreases and thinning behavior turns to thickening. The "ceramization" of the slurry flux steps up at the 50 vol.% suspensions. In fact, the 50TiCN at 45 vol.% slurry still behaves as the 430L suspension, while the flow curve of the 50TiCN at 50 vol.% follows a similar trend than the TiCN slurry.

The flow curves of the 430L, the TiCN and the mixtures (50TiCN, 60TiCN and 70TiCN) were fitted to the Cross model (Eq. 1). The Cross model allows to extrapolate the viscosity values for shear zero (η_0) and infinite (η_∞). The fitting was carried out about using the control stress curves for calculating the η_0 value, and using the control rate curves to determine the η_∞. Fig. 6 shows an example of the fittings done for the 430L, the 50TiCN and TiCN slurries at both solid loadings, while Table 1 collects the value of η_0, η_∞, and η_{100} (viscosity for 100 s^{-1} shear rate) for the tested suspensions. The η_0 is a value of the stability of the suspensions at rest; the higher is the viscosity the greater is the stability against the sedimentation and/or the segregation of the phases, which regularly takes place due to differences on densities and/or particle sizes. In our

Fig. 6. The log–log plots for the flow curves of 430L, TiCN and 50TiCN slurries with (a) 45 vol.% and (b) 50 vol.% solid contents. Dotted lines show as an example, how the approximations were done in order to determine the characteristic parameters η_0 and η_∞, as well as the value of the viscosity at 100 s^{-1}, η_{100}, collected in Table 1 for all prepared slurries.
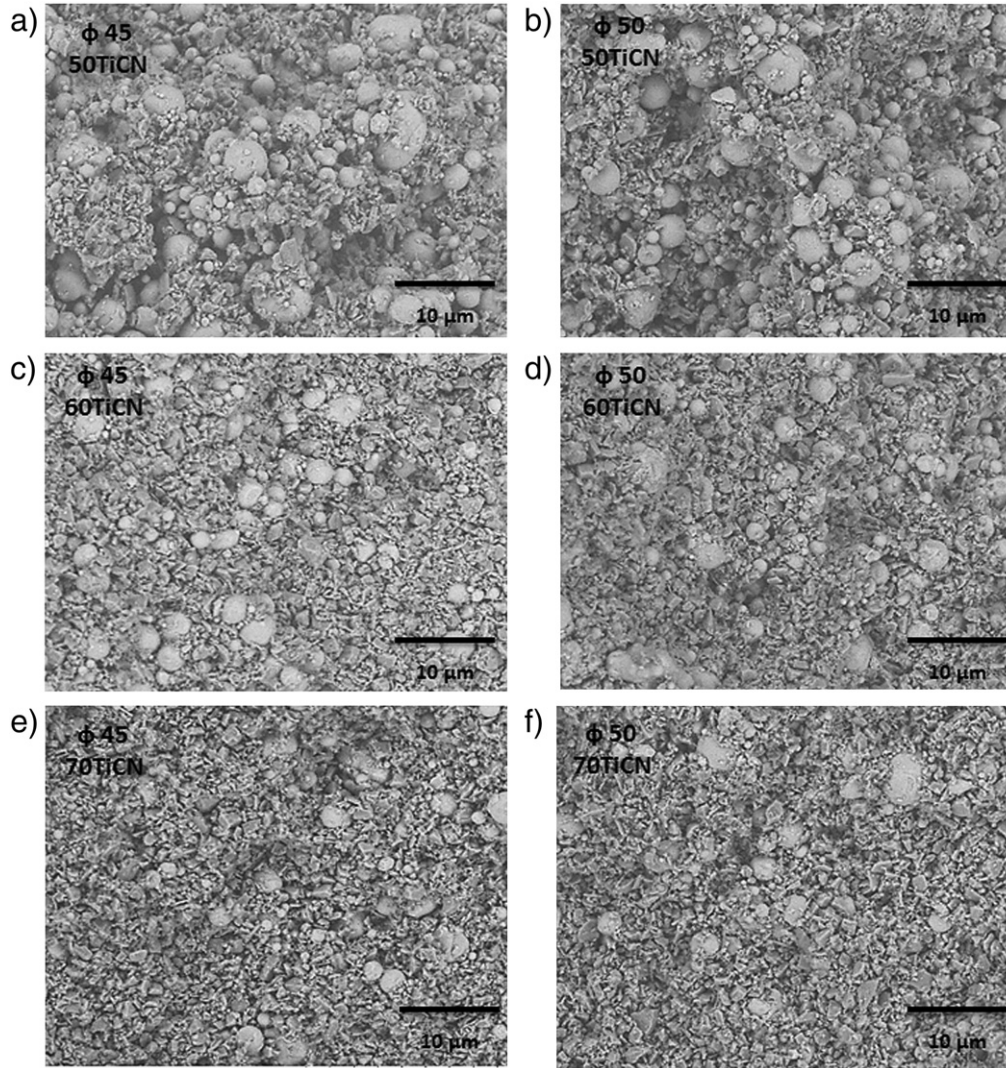
Fig. 7. SEM micrographs of the fracture surface of the green samples shaped by slip casting of 45 and 50 vol.% slurries of the three mixtures: (a) 50TiCN at 45 vol.%, (b) 50TiCN at 50 vol.%, (c) 60TiCN at 45 vol.%, (d) 60TiCN at 50 vol.%, (e) 70TiCN at 45 vol.% and (f) 70TiCN at 50 vol.%.

case, the ceramic phase, Ti(C,N), has a lower density (5.10 g/cm³) and also lower mean particle size (2 μm), if compared with 430L powder (7.7 g/cm³ and 11 μm). Those differences could promote the segregation by metal particle sedimentation during casting. Consequently, the η_0 is a relevant parameter which should be controlled and optimized for shaping homogeneous composites. The physical meaning of η_∞ is related with the stability of the suspensions for high shear rates, determining the efficiency of the milling or the stirring methods. Indeed, it infers in the preparation of homogeneous suspensions especially for powder mixtures.

Suspension parameters collected in Table 1 quantify how the addition of Ti(C,N) particles decreases the viscosity of the slurries and their yield stresses due to the bimodal particle size distribution resulting from the mixture of both powders (Fig. 2) [23]. Regularly, the incorporation of a large amount of the fine fraction of Ti(C,N) particles promotes a better flow, except in the case of 60TiCN slurries, where the synergic effect of both particle populations leads to the slurry thickening for both tested solid loadings.

Related to rheological parameters, most of the slurries have an adequate viscosity for casting ($\eta_{100} < 100$ mPa s). Only the 50 vol.% 430L slurry and both 60TiCN slurries could present difficulties during the shaping process. The η_0 values of 50TiCN and 70TiCN slurries are lower than the monophasic ones, increasing with the solid content. But all of measured η_0 values are enough to preserve the slurry from phase segregation [23]. In relation to the η_∞ values of the biphasic

slurries, the 50TiCN suspensions show the lowest values of η_∞ for both solid contents, so this composition collects the best rheological characteristics for homogenization and casting avoiding segregation.

3.3. Processing of composites with different 430L/Ti(C,N) rate

Bulk pieces of different 430L/Ti(C,N) compositions were obtained from the slurries by slip casting. After shaping (Fig. 1), the casted pieces were dried for 24 h at room temperature, and then characterized. Fig. 7 shows the microstructure of the green bulk pieces of the three compositions tested (50TiCN, 60TiCN and 70TiCN) for the two different solid contents (45 and 50 vol.%). The micrographs correspond to an unpolished random fracture surface for each composition.

Table 2
Green and sintered densities and hardness of the bulk pieces.

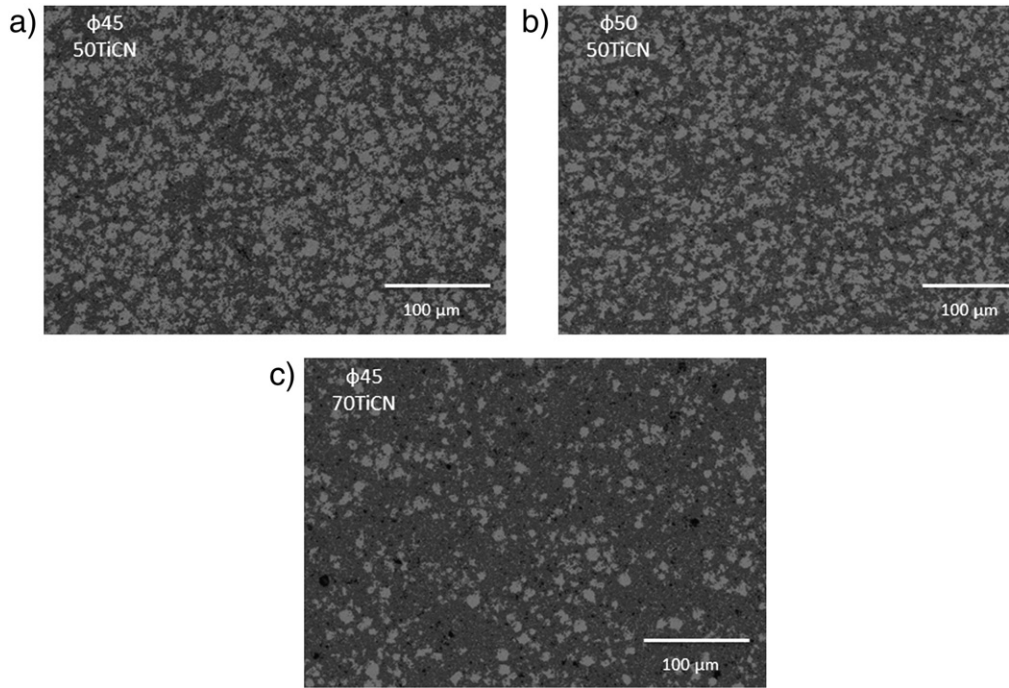| Solid loading		50TiCN	60TiCN	70TiCN
45 vol.%	%ρ_{green}	64%	60%	63%
	%ρ	98%	91%	94%
	HV30	520	567	932
50%	%ρ_{green}	66%	62%	64%
	%ρ	98%	90%	96%
	HV30	652	760	960

Fig. 8. SEM micrographs of the microstructure of sintered bulk pieces shaped by slip casting of the samples prepared from slurries (a) 50TiCN at 45 vol.%, (b) 50TiCN at 50 vol.%, and (c) 70TiCN at 45 vol.%.

It can be observed in Fig. 7 that the spherical 430L and the irregular-in-shape Ti(C,N) particles are homogeneously dispersed in all samples, such that the different compositions can be easily identified. That verifies that the η_0 values of all biphasic slurries (ranging from 0.89 to 9.74 Pa s in Table 1) are enough to avoid any particle settling. In all cases, the suspension stability is enough to avoid segregation of the phases at rest.

Table 2 summarizes the green and sintered densities of the bulk pieces, as well as the hardness values. The green density can be related with the degree of packing and the rheology of the suspensions: for a constant solid content, the higher viscosity of the suspensions the lower the green density of the casted pieces. The elevated viscosity of the 60TiCN slurries (>100 mPa s in Table 1) leads to a significant low value of the green density for both solid loadings. On the other hand, the increase of the solid content from 45 vol.% to 50 vol.% results in a 2% increase of the relative green density for the three compositions.

The green parts were sintered in a vacuum furnace (10^{-5} atm) at 1450 °C during 1 h. Reached temperature is enough to get a liquid phase of 430L wetting Ti(C,N) particles during the sintering [21]. All the sintered parts have metallic brightness. The values of hardness are higher when the parts were shaped from 50 vol.% slurries, as well as the density values, except for the 60Ti(C,N) pieces. However, although the low packing degree of 60Ti(C,N) green samples leads to a poor density of the composites after sintering (90–91%), the hardness increases with the amount of Ti(C,N) in all cases. The relative increment in hardness for the samples obtained through slurries with 50 vol.% solid content compared to 45 vol.% is about 20%, 25% and 3%, for the 50TiCN, 60TiCN and 70TiCN compositions, respectively.

Comparing with data collected in the literature, recently P. Alvaredo et al. [18], reported the value of density and hardness for a 430L/Ti(C,N) cermet with 50/50 *v/v* composition processed by powder metallurgic techniques. In this work, composites have 99% of relative density and 535HV30. Comparing those results with these reported here for similar powders and compositions, but shaped by colloidal processing, the density of the materials prepared by slip casting is slightly lower than by powder pressing (98%). However, in the case of the bulk pieces obtained from 50 vol.% slurries, composites are harder (652HV30) than those obtained by powder processing. Changes in hardness at similar, or even lower densities, could be a consequence of the more homogeneous distribution of the ceramic reinforcement (Ti(C,N)) in the metal matrix when materials are processed through a colloidal suspension. On the other hand, the hardness increases with the incorporation of the ceramic phase, as well as with the density of the final compact. Hardness achieves values of 932–940HV30 for cermets of 70/30 *v/v* Ti(C,N)/430L.

Fig. 8 shows the representative microstructures of 50TiCN at both solid contents and 70TiCN at 45 vol.%. Micrographs show that two different phases can be distinguished in the composites: a metallic gray phase corresponding to the 430L and the darkest phase of Ti(C,N). The black areas are pores. The porosity observed at the micrographs does not correspond with the values of density in Table 2. In fact, those pores, square in shape, corresponds to the pull out of small grains of
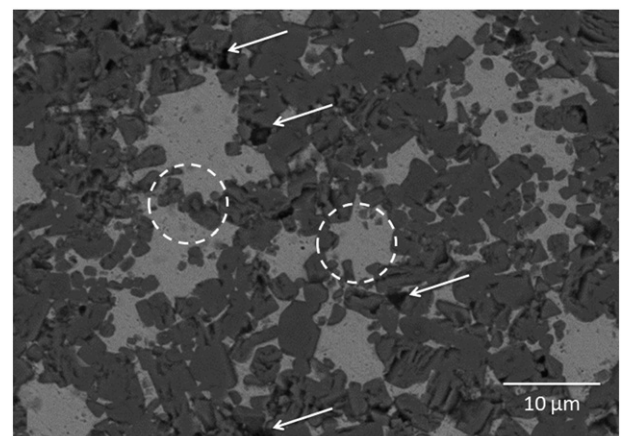

Fig. 9. SEM micrograph of 70TiCN compacts shaped from the 50 vol.% slurry. Arrows point out the presence of pull out holes due to the polishing, and the circles show metal and ceramic grains, and the stainless steel completely embedded the Ti(C,N) grains. The inset shows a photograph of the 70TiCN bulk piece with metal luster.
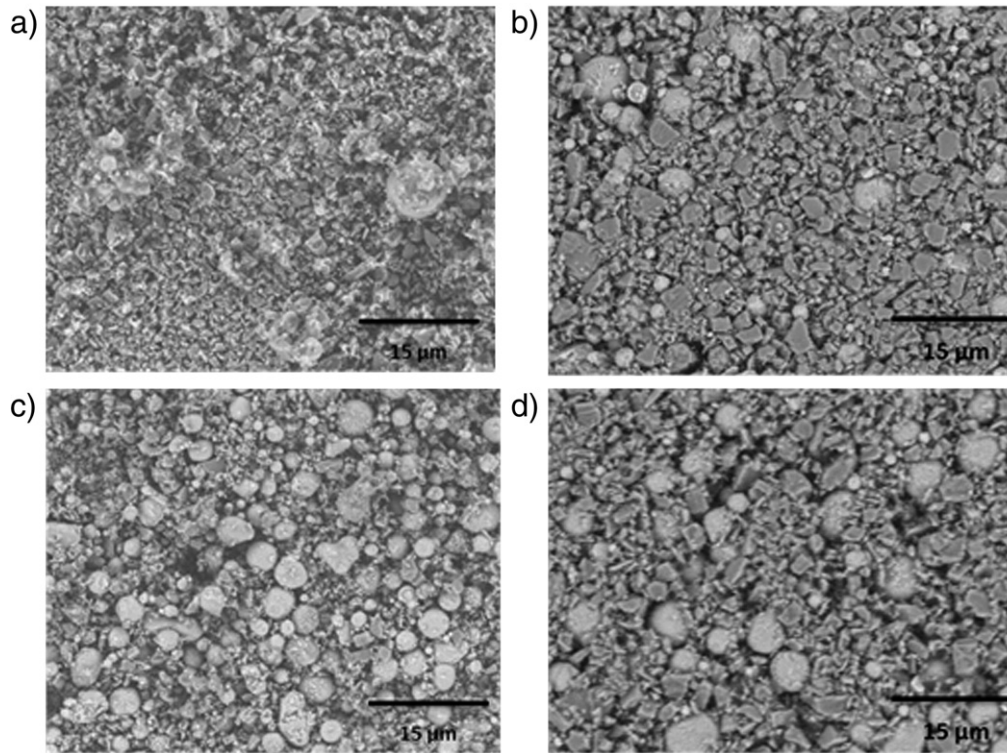
Fig. 10. SEM micrographs of the top and the bottom surfaces of the green FGM shaped by slip casting of 45 and 50 vol.% slurries of the 50TiCN slurry: (a) top surface for the 45 vol.% slurry, (b) top surface for the 50 vol.% slurry, (c) bottom surface for the 45 vol.% slurry and (d) bottom surface for the 50 vol.% slurry.

Ti(C,N) during polishing. All microstructures in Fig. 8 exhibit a homogenous and high dispersion degree of the two phases, noting that the mixture achieved the level of the particle size of the 430L and Ti(C,N) particles. That means, the particles in the composite are mixed one-by-one corroborating the high hardness values. This feature, as well as characteristic pull out of the hard phase, can be also observed at a higher magnification in the 70TiCN microstructure shown in Fig. 9. In this figure, the pores caused during polishing are shown as well as the size of the metal matrix among ceramic particles, which is similar to that of the starting powders. Ti(C,N) particles are surrounded by the stainless steel phase, which gives to the whole piece a metallic appearance despite the high ceramic content within the composite as is shown in the photograph at the inset. The degree of homogeneity of the mixtures noticed at this micrograph supports the increase of harness, but also supports the idea of the consolidation of a strengthened microstructure.

3.4. Processing of FGM samples with 50% v/v

Considering the results obtained in the monolithic bulk pieces described above for comparative proposes, the 50TiCN slurries were selected to shape FGM structures expecting to develop gradients of Ti(C,N) over a 50 vol.% in the cermet microstructure. As mentioned above, the 50TiCN slurries prepared at both solid loadings, 45 and 50 vol.%, exhibit an excellent rheology for the aim of this work. At both solid loadings, slurries have low and similar η_∞ values (4 to 3 mPa s) which assure a good homogenization of the mixture of the two powder fractions. They have an adequate viscosity for casting (57–72 mPa s) which leads to a similar density after the thermal treatment (98%). However, they exhibit differences in the η_0 parameters, the η_0 for 45 vol.% suspensions being 0.89 Pa s and the η_0 of 50 vol.% slurries 9.64 Pa s.

To prepare the FGM, a magnet was placed under the porous cast as shown in Fig. 1. The objective is to promote the migration of the 430L particles under the action of the magnetic field. Slurries were casted up to obtain rods 12 mm in highness and 8 mm in diameter (Fig. 1). The NdFeB magnet was placed under the porous cast for different times during shaping, in order to evaluate the migration of the 430L throughout the slurry. Slides of 2 mm in highness were cut from the top and the bottom of each sample. In this way, the composition of both edges of the as-casted FGMs at different times was evaluated, and then the gradation of the composition was determined. Fig. 10 shows the microstructure of the top and the bottom of the green pieces prepared placing the magnet for 1 h during casting the 45 vol.% slurry (a and c) and for 15 h the 50 vol.% (b and d) slurry.

Microstructures in Fig. 10 show that there is a slight difference in the amount of 430L particles when 50 vol.% slurries are considered, while this difference augments between the top and the bottom-slides when bulk pieces were shaped from the 45 vol.% slurry. Results evidence the migration of 430L particles under the effect of the applied magnetic field. The migration of metal particles can be related to the values of η_0 of the slurries. The lower η_0 value of the 45 vol.% slurry (0.89 Pa s) promotes the faster migration of 430L particles, while the high viscosity that the 50 vol.% suspension exhibits at rest (9.64 Pa s) retards the segregation of phases under the magnetic field. So, the micrographs of the top and bottom-slides evidence that differences in the rheology behavior of the suspensions determine the gradient gap in composition of the FGM, and limit the process viability.

Table 3
Values of the density and open porosity of the FGM top and bottom-slides and the full density, calculated without regarding the open porosity.

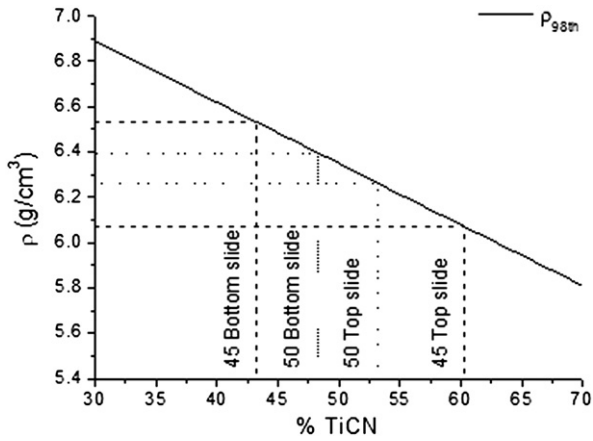| Solid content	Slide	Density (g/cm^3)	Open porosity	Density of the structure (g/cm^3)
45 vol.%	Top	6.07	0%	6.07
	Bottom	6.22	5%	6.53
50 vol.%	Top	5.80	12%	6.50
	Bottom	5.92	8%	6.39

Fig. 11. Plot of the density vs Ti(C,N) content for the FGM shaped from 45 and 50 vol.% slurries.

To determine the amount of Ti(C,N) at the edges of the FGM, two different techniques were used: the image analysis and the difference on densities between the top slide and the bottom slide cut from the FGMs. Densities of the top-slide and the bottom-slide were measured by water immersion technique which allows determining the density of the cermet structure despite the open porosity of the sample. Table 3 shows the values of the density of the top and bottom slides for both FGMs, its open porosity and the calculated values of the density without regarding the open porosity.

In view of the high density (98%) of 50TiCN bulk pieces, prepared for both solid loadings, and considering that during sintering the metal phase melts while the ceramic phase is no sintered, we can refer the 2% of porosity to the ceramic phase. In Fig. 11 the plot shows the evolution of the theoretical density (following the law of mixtures) as a function of the Ti(C,N) volume fraction calculated for a 2% of porosity of the ceramic phase. This calibration line was used to determine the volume fraction of Ti(C,N) which corresponds to the densities measured for the top and the bottom slides of both FGMs. The concentration of Ti(C,N) varies from 60% to 43% at the FGM prepared from the 45 vol.% slurry, while in the case of the FGM obtained from the 50 vol.% slurry, the variation of the Ti(C,N) content ranges from 48% to 53%. The low gradient obtained at the 50 vol.% FGM is due to the high viscosity at rest (η_0). Table 4 summarizes the collected data about the Ti(C,N) content from the image analysis and the determination of densities of the top and bottom slides, as well as the values of hardness.

The results of the image analysis fit those obtained when measuring the density of different pieces of the FGM. The gradient of Ti(C,N) along the 12 mm of the FGM is 17% for the 45 vol.% slurry and 5–6% for the 50 vol.%. The hardness values obtained for the two slides for the 45 vol.% FGM are higher than the estimated hardness from the data of the composite monolithic parts in Table 2. However, in the case of the FGM prepared from the 50 vol.% slurry, the hardness values obtained in both slides are lower than the estimated values. This can be related to the higher viscosity of this slurry and the lower homogeneity of the

structure after the magnetic shaping. Hardness values are in good agreement with the estimated Ti(C,N) content by image analysis and the density determination.

The difference among hardness values registered at the monolithic sample and the FGM reveals that the re-accommodation of particles during packing also promotes the hardening of the FGM microstructure obtained from the 45 vol.%. The porosity of both extremes was determined (Table 3). The top-slide has no open porosity, while the bottom slide has a 5% open porosity. Fig. 12 shows the micrographs of the top-slide (a and c) and the bottom-slide (b and d) of the FGM. If compared with the microstructures of the monolithic bulk pieces (Fig. 9), the metal content corresponds to the registered values collected in Table 4. However, the distribution of the reinforcement within the metal matrix seems to correspond to mixtures of different particle sizes.

As shown in Fig. 12 a, the microstructure of the top slide at lower magnification presents a high distribution of the phases without large areas of 430L which implies that both phases have similar sizes. This similitude between the particle sizes is corroborated in the micrograph at a higher magnification (Fig. 12 c), where the 430L areas are smaller than the dv50 of the particle (<11.5 μm). Moreover, in the case of the bottom slide, it is easy to see in Fig. 12 b that the Ti(C,N) particles are concentrated in the edge of larger 430L areas. In Fig. 12 d it can be observed that these areas are larger than the dv50 of the 430L (>11.5 μm). This confirms the difference in the distribution of the 430L particle size, between the top slide and bottom slide, promoted by the magnetic migration of the larger metal particles. This magnetic migration results in more homogeneous structures by narrowing the particle size distribution at both ends enhancing the hardness.

4. Conclusions

Cermets of 430L/Ti(C,N) with a graded microstructure was shaped in a one-step process through colloidal techniques. The migration through the slurry during casting of 430L particles under the effect of a magnetic field favors the formation of a continuous gradient in composition. This gradient depends on the viscosity of the suspension at rest, η_0. A continuous gradient of 17% and 5% in Ti(C,N) along the bulk piece (12 mm) can be promoted from 45 and 50 vol.% slurries, respectively. During the generation of the gradient, the coarse 430L particles are mostly attracted by the magnetic field promoting also the segregation of the metal particles according to its size. This effect results in more homogeneous microstructures at the top and the bottom of the FGM, which improves hardness. Experimentally, the determining factor in the processing of these materials by colloidal techniques is the η_0. This parameter limits not only the gradient but also the homogeneity of the structure, and then its hardness.

The Ti(C,N) powders have been homogenously dispersed in a metal matrix of 430L stainless steel. Both phases are mixed in the range of their particle sizes. Monolithic composites with properties even higher (in hardness) than those obtained by powder metallurgy techniques were produced. The homogeneity of the dispersion and the micrometric size of the powder allows the processing of cermets with 70 vol.% of Ti(C,N) in composition with metallic luster.

Table 4
Calculation of the %Ti(C,N) in FGM and hardness values.

| | %Ti(C,N) | | | | Hardness (HV30) | | | |
| | From density estimation | | From image analysis | | Experimental | | Estimated[a] | |
	45%	50%	45%	50%	45%	50%	45%	50%
Top slide	60%	53%	58%	52%	607	592	567	668
Bottom slide	43%	48%	41%	46%	418	541	315	591
Difference	17%	5%	17%	6%				

[a] Those data have been estimated from the hardness values measured for the monolithic rods.
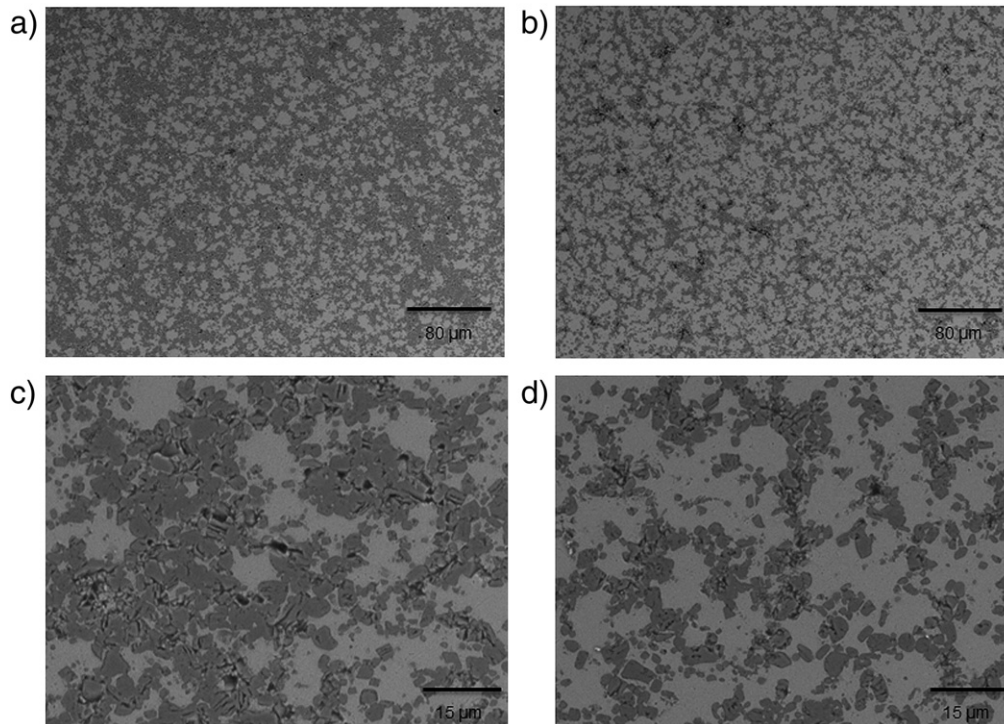
Fig. 12. SEM micrographs of top slide (a) and bottom slide (b) at lower magnifications and a magnification of the microstructure of the top (c) and bottom (d) of the FGM prepared from 45 vol.% slurries.

Acknowledgment

References

[1] Gu P, Asaro RJ. Cracks in functionally graded materials. Int J Solids Struct 1997;34(1):1–17.

[2] Kieback B, Neubrand A, Riedel H. Processing techniques for functionally graded materials. A paper from the German Priority Programme (functionally graded materials). Mater Sci Eng 2003;362(1-2):81–106.

[3] Eso O, Fang Z, Griffo A. Liquid phase sintering of functionally graded WC–Co composites. Int J Refract Met Hard Mater 2005;23(4-6 SPEC. ISS):233–41.

[4] Fan P, Fang ZZ, Guo J. A review of liquid phase migration and methods for fabrication of functionally graded cemented tungsten carbide. Int J Refract Met Hard Mater 2013;36:2–9.

[5] Konyashin I, Ries B, Lachmann F, Fry AT. Gradient WC–Co hardmetals: theory and practice. Int J Refract Met Hard Mater 2013;36:10–21.

[6] Lengauer W, Dreyer K. Tailoring hardness and toughness gradients in functional gradient hardmetals (FGHMs). Int J Refract Met Hard Mater 2006;24(1–2):155–61.

[7] Shi Z, Feng P, Liu W, Zheng Y, Li J. Tribological behavior of Ti(C, N)-based and functionally gradient Ti(C, N)-based cermets. 97-101 ed. Zhuhai: Advanced Materials Research; 2010 1097–103.

[8] Zhong J, Zheng Y, Zhang Y. Fabrication technology of functionally graded Ti(C, N)-based cermets. Fuhe Cailiao Xuebao/Acta Materiae Compositae Sinica 2009;26(3):111–5.

[9] Konyashin I. A technique for fabrication of coated TiCN-based cermets with functionally graded structure. Int J Refract Met Hard Mater 2001;19(4–6):523–6.

[10] Garcia J, Pitonak R. The role of cemented carbide functionally graded outer-layers on the wear performance of coated cutting tools. Int J Refract Met Hard Mater 2013;36:52–9.

[11] Hernández N, Sánchez-Herencia AJ, Moreno R. Forming of nickel compacts by a colloidal filtration route. Acta Mater 2005;53(4):919–25.

[12] Escribano JA, Ferrari B, Alvaredo P, Gordo E, Sánchez-Herencia AJ. Colloidal processing of Fe-based metalceramic composites with high content of ceramic reinforcement. Bol Soc Esp Cerámica Vidrio 2013;52(6).

[13] Hernández N, Moreno R, Sánchez-Herencia AJ, Fierro JLG. Surface behavior of nickel powders in aqueous suspensions. J Phys Chem B 2005;109(10):4470–4.

[14] Guo Z, Xiong J, Yang M, Xiong S, Chen J, Wu Y, et al. Dispersion of nano-TiN powder in aqueous media. J Alloys Compd 2010;493(1–2):362–7.

[15] Shih C-J, Lung B-H, Hon M-H. Colloidal processing of titanium nitride with poly-(methacrylic acid) polyelectrolyte. Mater Chem Phys 1999;60(2, Lausanne, Switzerland):150–7.

[16] Sánchez-Herencia AJ. Water based colloidal processing of ceramic laminates. 333 ed. Key Engineering Materials; 2007 39–48.

[17] Gauckler LJ, Graule T, Baader F. Ceramic forming using enzyme catalyzed reactions. Mater Chem Phys 1999;61(1):78–102.

[18] Alvaredo P, Tsipas SA, Gordo E. Influence of carbon content on the sinterability of an FeCr matrix cermet reinforced with TiCN. Int J Refract Met Hard Mater 2013;36:283–8.

[19] Kosacheva EM, Kudryavtsev DB, Bakeeva RF, Kuklin AI, Islamov AKh, Kudryavtseva LA, et al. The aggregation of branched polyethylenimine and cationic surfactants in aqueous systems. Colloid J 2006;68(6):713–20.

[20] Lewis JA. Colloidal processing of ceramics. J Am Ceram Soc 2000;83(10 Westerville, OH, United States):2341–59.

[21] Sigmund WM, Bell NS, Bergström L. Novel powder-processing methods for advanced ceramics. J Am Ceram Soc 2000;83(7 Westerville, OH, United States):1557–74.

[22] Wyss HM, Tervoort EV, Gauckler LJ. Mechanics and microstructures of concentrated particle gels. J Am Ceram Soc 2005;88(9):2337–48.

[23] Sánchez-Herencia JA, Hernández N, Moreno R. Rheological behavior and slip casting of Al$_2$O$_3$–Ni aqueous suspensions. J Am Ceram Soc 2006;89(6):1890–6.